Structures 60 (2024) 105828

Contents lists available at ScienceDirect

Structures

journal homepage: www.elsevier.com/locate/structures

Residual stresses in steel I-sections strengthened by wire arc additive manufacturing

P. Kyvelou, C. Huang *, J. Li, L. Gardner

Department of Civil and Environmental Engineering, Imperial College London, UK

ARTICLE INFO

Keywords:
3D printing
Experiments
Residual stresses
Residual stress pattern
Sectioning method
Strengthened I-sections
Tests
Wire arc additive manufacturing

ABSTRACT

Wire arc additive manufacturing (WAAM) is a method of metal 3D printing that can be used to complement traditional steel manufacturing techniques (e.g. hot-rolling and cold-forming), to produce hybrid structural elements of enhanced efficiency. The case of hot-rolled steel I-sections strengthened by the addition of WAAM stiffeners at the flange tips is the focus of the present study. In addition to the improved local buckling resistance and increased flexural rigidity achieved by the addition of the stiffeners, a further source of enhanced load-bearing capacity arises from the inversion, through thermal action, of the adverse residual stress pattern typically associated with hot-rolled I-sections. Thus, in contrast to previous studies, the aim of the present investigation is not to eliminate but to take benefit from residual stresses, by prestressing (pretensioning) specific parts (i.e. the flange tips) of steel sections against subsequent applied compressive loading, thereby delaying yielding and enhancing the load-bearing capacity. The described hypothesis is demonstrated in the present study through the manufacture of a series of hybrid WAAM-strengthened hot-rolled I-sections and the subsequent performance of residual stress measurements. Stiffeners of different dimensions were printed using ER70S-6 welding wire. A detailed description of the adopted experimental technique, which utilised the sectioning method, is provided, while the magnitude and distribution of the measured residual stresses are reported. The addition of WAAM stiffeners at the flange tips of hot-rolled I-sections is shown to lead to the generation of desirable (for structural stability) tensile residual stresses in their vicinity, with peak values reaching the yield strength of the material; self-equilibrating compressive residual stresses are induced in the web and around the web-to-flange junction.

1. Introduction

Residual stresses are stresses that exist within steel structural members in the absence of external loading; these stresses are self-equilibrating and are typically induced in steel elements during the production process. Non-uniform plastic deformations are the key cause of residual stresses in cold-formed sections [26,27], while in hot-rolled and welded sections, residual stresses are induced mainly through temperature gradients, arisen from uneven cooling and localised welding heat input, respectively [35,41,11,10]. Residual stresses generally have an adverse influence on the structural stability and ultimate capacity of steel I-section columns and beams, with the compressive residual stresses at the flange tips causing premature yielding and loss of flexural stiffness.

Wire arc additive manufacturing (WAAM) is a metal 3D printing method that utilises arc welding coupled with robotics to build parts through the incremental layer-by-layer deposition of material [20,19,23,25]. WAAM is deemed to be well-suited for use in construction, since it enables the efficient and economic production of large and complex structural parts, opening up opportunities for structural strengthening and repair [16,9]. The high heat input and repetitive thermal cycles during WAAM can induce high residual stresses in the built parts, which often lead to distortion, thus decreasing the geometric precision of the products [18,22]. Hönnige et al. [17] examined the residual stress patterns in WAAM aluminium walls by means of neutron diffraction, finding the residual stresses to range from 60% to almost 100% of the material yield strength and to be predominantly in the print layer direction. Ding et al. [5] revealed significant residual stresses and distortion in WAAM mild steel walls, with longitudinal residual stresses exceeding the material yield strength. Given their significance and typically detrimental effects, the elimination or mitigation of residual stresses in WAAM parts has been the subject of extensive research. Xiong et al. [37] showed that preheating the substrate could somewhat relieve the residual stresses in thin-walled WAAM parts, while Colegrove et al.

* Corresponding author.
E-mail address: cheng.huang118@imperial.ac.uk (C. Huang).

https://doi.org/10.1016/j.istruc.2023.105828
Received 9 September 2023; Received in revised form 30 November 2023; Accepted 23 December 2023
Available online 5 January 2024

Table 1
Chemical composition of ER 70S-6 welding wire (% by weight, balance Fe).

C	Si	Mn	S	P	Cu	Ni	Cr	Mo
0.071	0.835	1.447	0.015	0.010	0.173	0.037	0.049	0.015

Al	V	Zr+Ti	N	Ti	Zr	Sn	As	B
0.002	0.002	0.009	0.006	0.008	0.001	0.009	0.003	0.001

Table 2
Mechanical properties of as-welded ER 70S-6 welding wire (as provided by manufacturer).

f_y (MPa)	f_u (MPa)	ε_f (%)	Impact energy (J)
470	570	26	80 @ −40 °C

Table 3
Printing parameters for WAAM stiffeners.

Process parameter	Value
Wire diameter (mm)	1.2
Torch travel speed (mm/s)	11
Voltage (V)	17
Current (A)	200
Wire feed rate (m/min)	6.0
Deposition rate (kg/h)	3.0
Average layer height (mm)	1.4
Average layer width (mm)	6.5

[2] and Martina et al. [24] found that post-rolling can significantly reduce residual stresses and distortion in WAAM parts. Post-deposition heat treatment e.g. induction heating [31] has also been shown to be capable of modifying the residual stresses distributions in 3D printed parts [14].

Residual stresses in WAAM or WAAM-strengthened elements can be determined by means of non-destructive and destructive techniques [36]. However, non-destructive measuring techniques, including X-ray diffraction, neutron diffraction and ultrasonic and magnetic methods, are generally less suitable for examining printed parts of the scale of structural members. Hole-drilling and sectioning are two common destructive methods, whereby residual stresses are determined based on the strains relieved upon the removal of material from the specimen. The hole-drilling method is often used to measure near-surface residual stresses, while the sectioning method, due to its effectiveness and simplicity, has been widely used to examine residual stresses in structural steel members [32,33,39,42].

In this paper, residual stress measurements on I-section steel columns strengthened by the addition of WAAM stiffeners at the flange tips are presented. The WAAM stiffeners were added to improve the performance of the I-sections through an increased cross-sectional area and second moment of area, enhanced local buckling capacity and a more favourable residual stress pattern. Specifically, the typical residual stress pattern in hot-rolled steel I-sections that features moderate (around 30–50% of the material yield strength) compressive residual stresses at the flange tips (with a detrimental effect on structural stability) is replaced by one that features high tensile residual stresses at the flange tips, with a positive effect on structural stability by delaying first yield. Thus, in contrast to previous studies, the aim of the present investigation is not to eliminate but to take benefit from residual stresses. Three structural steel I-sections strengthened with WAAM stiffeners of two different nominal heights, together with a reference bare specimen, were examined. The sectioning method, implemented using waterjet cutting, was employed to investigate the levels and distributions of residual stresses in the WAAM-strengthened (and bare) hot-rolled steel I-sections, aided by complementary material tests. A description of the adopted experimental techniques is provided, while the magnitude and distribution of the residual stresses are presented and analysed.

2. Specimen design and manufacture

Hot-rolled S355 steel UC 152 × 152 × 23 profiles were examined in the present study, with stiffeners of different nominal heights added to the flange tips by means of WAAM. Carbon steel welding wire of grade ER 70S-6 (EN ISO 14341-A G 42 3 M21 3Si1 in line with EN ISO 14341 [7]) and of 1.2 mm diameter was used as the feedstock material for the manufacture of the stiffeners; the chemical composition and key mechanical properties of the employed welding wire, as specified by the manufacturer, are provided in Tables 1 and 2 respectively, where f_y is the yield strength, f_u is the ultimate tensile strength and ε_f is the percentage elongation at fracture. For each specimen, a total of four stiffeners were added, printed one by one, with the two on the same flange printed first, followed by the other two on the second flange, to limit the thermal distortion of the member during printing. The key printing parameters are presented in Table 3; note that the deposition rate was calculated excluding the dwell time between layers. A total of three WAAM-strengthened specimens were manufactured and subjected to residual stress measurements, while a bare specimen was also examined to provide a reference residual stress pattern.

Following manufacture, all specimens were first wire brushed and cleaned with acetone, and then laser scanned to determine their geometric properties. A FARO Scan Arm, capable of capturing 600,000 points per second with an accuracy of ± 0.075 mm, was used to obtain the point cloud of the scanned specimens, which was subsequently converted into a polygon mesh using the software [13]) and imported into Rhino [28] for geometric analysis – see Fig. 1. Note that, since direct scanning of the inner surface of the WAAM stiffeners was not possible due to the obstruction of the web, the inner surface geometry was estimated using a curvature-based hole-filling function in Geomagic Wrap [13]. It should be mentioned that the cross-sectional dimensions determined by means of laser scanning were verified against sample Vernier calliper measurements.

The average cross-sectional dimensions of the specimens, namely the height H, breadth B, flange thickness t_f, web thickness t_w, fillet radius r and average height h_s and width w_s of the WAAM stiffeners are defined in Fig. 2 and reported in Table 4. The adopted labelling system for the residual stress specimens starts with the letter B to denote the bare steel section or S for the WAAM-strengthened sections. For the three strengthened specimens, the S is followed by the nominal height of the WAAM stiffeners in mm; one of the strengthened specimens had 8 mm stiffeners (S-8), while the other two had 24 mm stiffeners (S-24a and S-24b). The bare I-section was used as a benchmark for the remainder of the specimens. All test specimens, including the bare and WAAM-strengthened I-sections, are shown in Fig. 3.

3. Material tests

The mechanical characteristics of both types of steel employed within the examined specimens (i.e. the hot-rolled section and the WAAM stiffeners) were determined by means of tensile coupon tests, undertaken at room temperature in compliance with EN ISO 6892–1 [8]. Dog bone shaped coupons were extracted from the strengthened columns by means of waterjet cutting. Six coupons were extracted from the

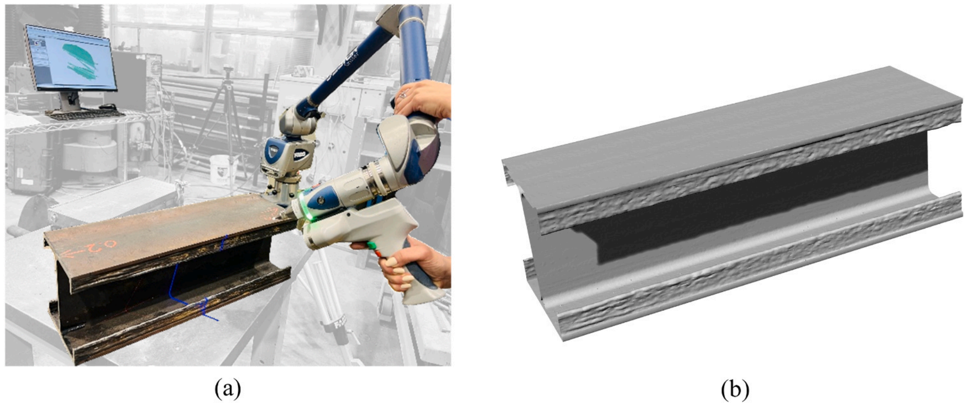

Fig. 1. (a) Laser scanning and (b) 3D CAD model of WAAM-strengthened I-section specimen.

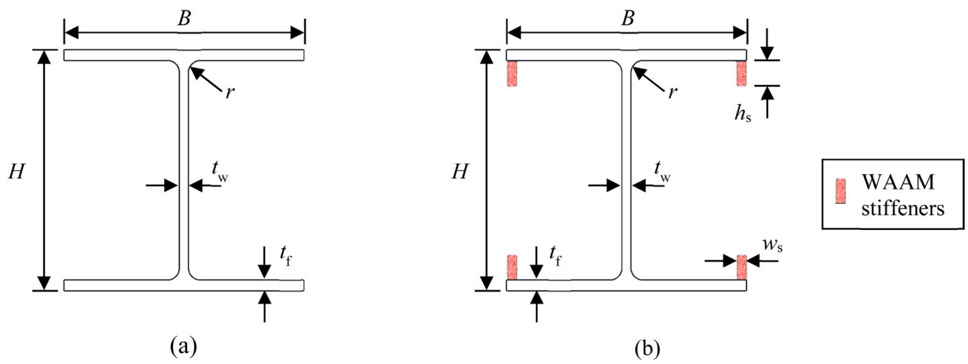

Fig. 2. Cross-sectional dimensions of (a) bare and (b) WAAM-strengthened I-sections.

Table 4
Average measured geometric properties of test specimens.

Specimen ID	H (mm)	B (mm)	t_f (mm)	t_w (mm)	r (mm)	h_s (mm)	w_s (mm)
B	152.54	151.97	6.45	6.01	12.18	-	-
S-8	151.90	152.45	6.75	6.06	10.36	8.18	6.59
S-24a	152.24	152.20	6.73	6.04	10.14	24.13	6.71
S-24b	152.19	151.59	6.77	6.04	10.18	24.29	6.35

flanges and web of the hot-rolled steel I-sections (i.e. four from the flanges and two from the web) and four from the WAAM stiffeners; ten coupons were tested in total. Subsequent to their extraction, all coupons were sandblasted with glass beads to clean their surface from rust and any welding soot remaining from the WAAM process – see Fig. 4(a). The nominal dimensions of the coupons, shown in Fig. 4(b), were specified in line with EN ISO 6892–1 [8].

The cross-sectional area A of the parallel length of the smooth coupons (i.e. those extracted from the hot-rolled sections) was determined based on measurements taken using Vernier callipers and a mechanical micrometre of 0.001 mm accuracy. For the coupons extracted from the WAAM stiffeners, since their undulating as-built surface, shown in Fig. 4 (a), rendered the use of conventional measuring tools impractical, 3D laser scanning was employed. The point cloud of the scanned coupons was converted into a polygon mesh using the software Geomagic Wrap [13] and imported into Rhino [28] for subsequent geometric analysis,

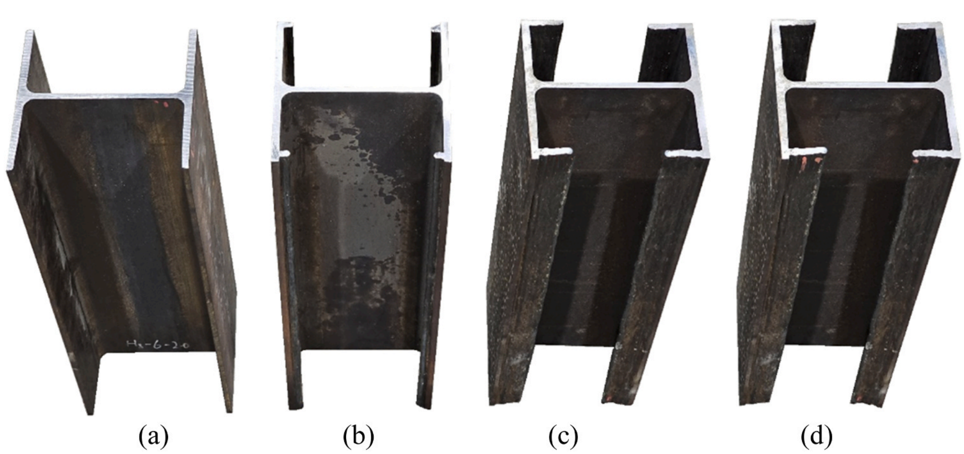

Fig. 3. Specimens for residual stress measurements: (a) B, (b) S-8, (c) S-24a, (d) S-24b.

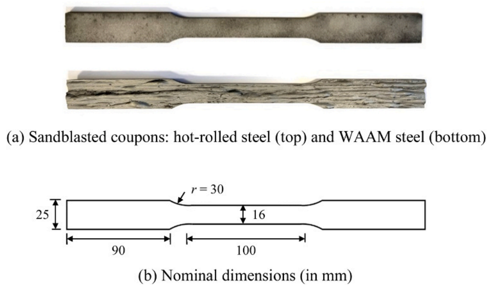

(a) Sandblasted coupons: hot-rolled steel (top) and WAAM steel (bottom)

(b) Nominal dimensions (in mm)

Fig. 4. (a) Typical sandblasted hot-rolled steel and WAAM coupons and (b) coupon dimensions.

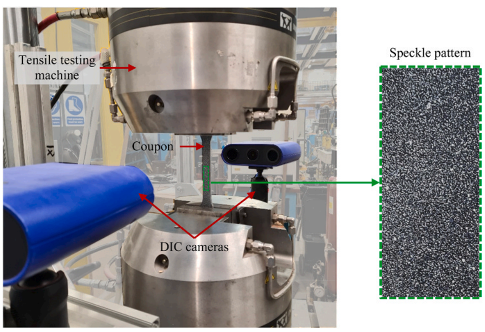

Fig. 5. Tensile coupon test setup.

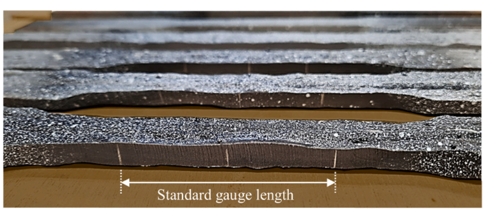

Fig. 6. Standard gauge length marked on the side of WAAM coupons.

following the process described by Huang et al. [21].

The tensile test setup is shown in Fig. 5. A four-camera LaVision digital image correlation (DIC) system was employed to monitor the strain fields during testing, with each camera pair monitoring opposite coupon faces. A random white speckle pattern on a matt black background was applied along the parallel length of both coupon faces, to allow the detection of deformations during image acquisition by the DIC system. A 250 kN Instron 8802 testing machine was used for the application of the tensile load, which was measured by a load cell within the actuator. The tensile load was applied using displacement control, with a slower strain rate of 0.00007 s^{-1} up to yield and a faster strain rate of 0.00025 s^{-1} post yield, and a gradual transition between them [8]. The acquisition of images was carried out at a frequency of 1 Hz, while the applied tensile load was recorded by the DIC system through an analogue to digital converter. The acquired images were processed in the software DaVis [4], and the strains were calculated using a virtual strain gauge placed over the full area of the parallel length. Standard gauge lengths were marked onto the coupons, as shown in Fig. 6, for the calculation of fracture strains ε_f [8].

The obtained engineering stress-strain curves are presented in Fig. 7(a), while their initial range is more clearly shown in Fig. 7(b). The mechanical properties obtained from the coupons extracted from the hot-rolled steel sections and the effective mechanical properties obtained from the coupons extracted from the WAAM stiffeners are presented in Tables 5 and 6 respectively, where E is the Young's modulus, f_y is the yield strength, f_u is the ultimate tensile stress, ε_u is the strain at the ultimate tensile stress and ε_f is the fracture strain measured over the standard gauge length. The mean and COV (coefficient of variation)

Table 5
Mechanical properties obtained from tensile coupons extracted from hot-rolled steel sections.

Coupon Label	E (MPa)	f_y (MPa)	f_u (MPa)	ε_u	ε_f
F1	212,700	423	569	0.143	0.367
F2	210,600	416	567	0.141	0.383
F3	209,500	414	561	0.149	0.400
F4	209,600	406	558	0.142	0.433
W1	211,300	414	572	0.145	0.327
W2	209,100	408	561	0.147	0.309
Mean	210,500	413	565	0.145	0.370
COV	0.006	0.013	0.009	0.018	0.114

Table 6
Effective mechanical properties obtained from tensile coupons extracted from WAAM stiffeners.

Coupon Label	E (MPa)	f_y (MPa)	f_u (MPa)	ε_u	ε_f
S1	208,400	415	535	0.150	0.309
S2	212,500	408	529	0.127	0.291
S3	214,700	409	527	0.109	0.350
S4	214,900	393	513	0.118	0.300
Mean	212,600	406	526	0.126	0.313
COV	0.012	0.020	0.015	0.119	0.072

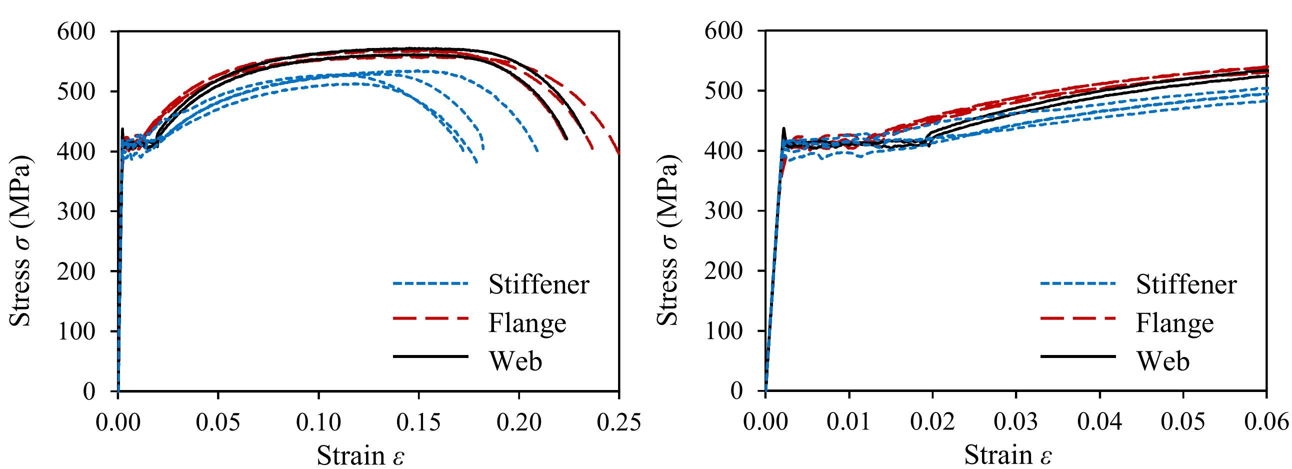

Fig. 7. Stress-strain curves obtained from tensile coupon tests: (a) full curves, (b) initial range.

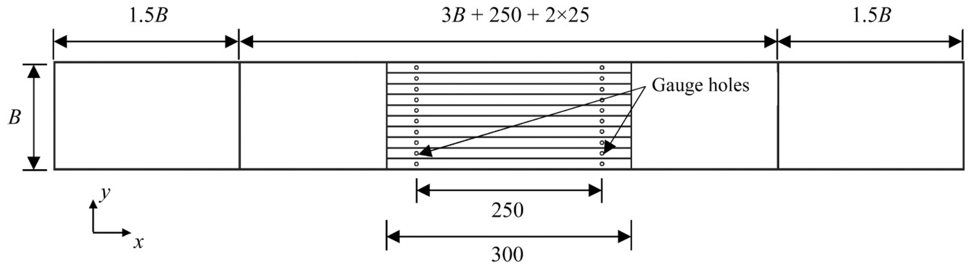

Fig. 8. Overall layout within member for residual stress measurements (dimensions in mm).

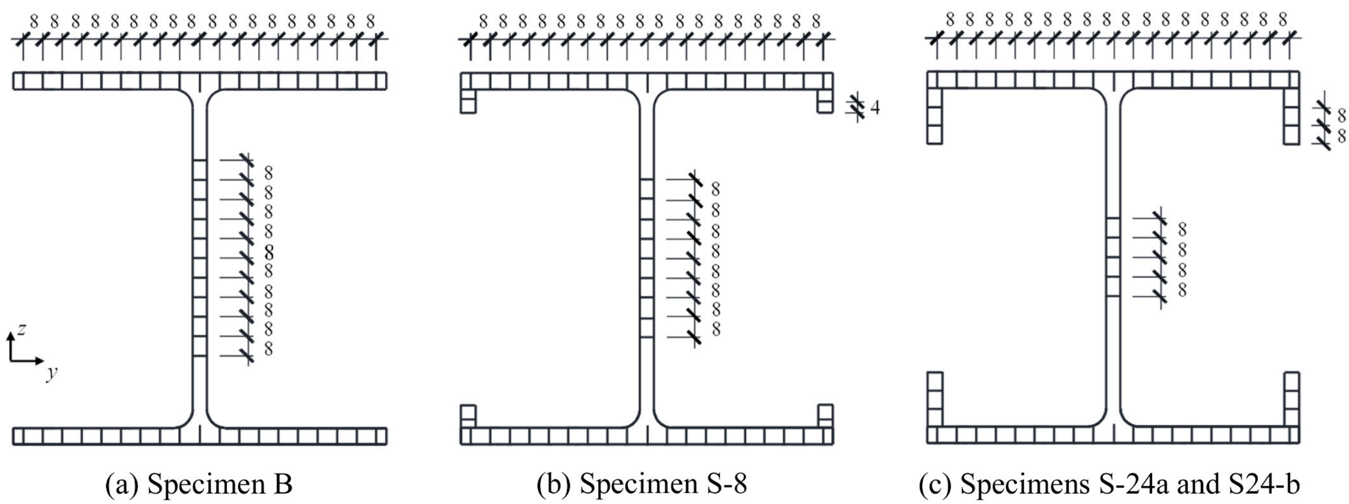

Fig. 9. Cross-sectional layout for residual stress measurements (locations of gauge holes are shown, with dimensions in mm).

values are also reported. Note that the mechanical properties obtained from the WAAM stiffeners are referred to as 'effective', since these values were determined based on the average cross-sectional area over the parallel length of the coupons and would have been influenced by the surface undulations inherent to the WAAM process. It has been shown in previous research [20,21] though that as-built coupons (i.e. those with the surface undulations present) tested along the print layer direction (as in the present study) exhibit similar mechanical properties to corresponding machined coupons (i.e. those with the surface undulations removed), with the reported differences in E, f_y and f_u being less than 3% [21]. The adopted labelling system for the tensile coupons begins with the letter F, W or S for the coupons extracted from the flange, web or WAAM stiffener respectively, followed by the test number.

4. Residual stress measurement technique

The sectioning method, which is the principal destructive technique used for the determination of residual stresses in structural members [29,34], was employed herein to measure the residual stresses in the examined cross-sections. The layout of the specimens within the member length is illustrated in Fig. 8, while the locations and dimensions of the strips within the cross-sections are shown in Fig. 9. Note that the specimens were fabricated to be sufficiently long to ensure that representative residual stress patterns would be included in the central 300 mm measurement region (see Fig. 8) and that end effects would be minimised [43].

Prior to sectioning, the strips were marked out on the specimens and pairs of 2 mm diameter gauge holes were drilled at their ends over a gauge length of 250 mm, using a CNC milling machine. The complete set of gauge holes for the flange of a typical specimen is shown in Fig. 10(a). The gauge holes were lightly sanded to remove any burrs from the drilling operations and cleaned with acetone and an air blast. In line with the recommendations of the Structural Stability Research Council [43], three repeated readings were taken on each pair of gauge holes using a Demec gauge, with the mean value recorded as the initial gauge

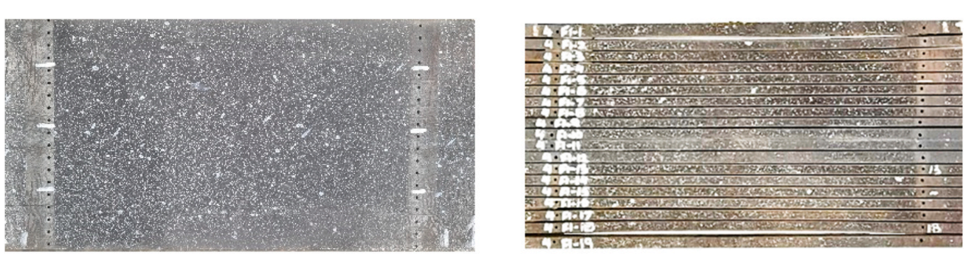

(a) (b)

Fig. 10. Steps of sectioning method: (a) gauge holes drilled in cross-section before initial measurements and (b) cross-section cut into strips by waterjetting before final measurements.

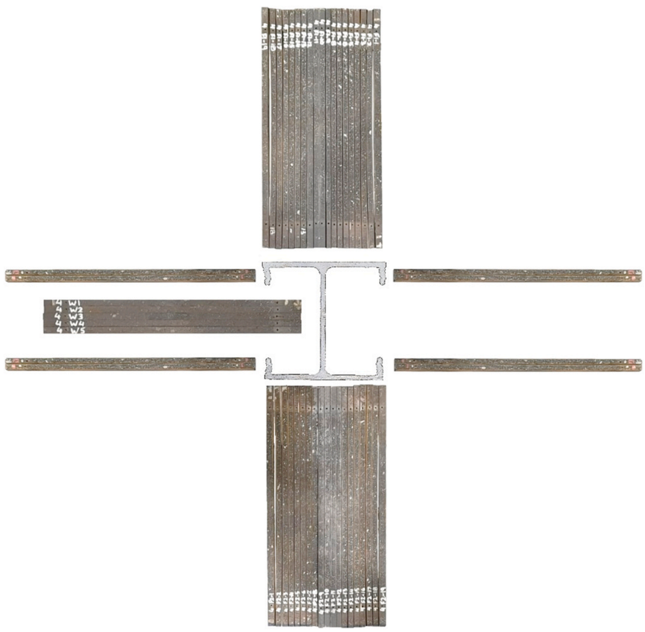

Fig. 11. Typical sectioned WAAM-stiffened specimen (Specimen S-24a).

length, denoted r_i. Note that readings were taken on both sides of each strip when this was possible (i.e. when positioning of the Demec gauge was not obstructed by the web-to-flange or flange-to-stiffener junctions). After the initial gauge length readings were taken, the marked strips were cut and subsequently extracted from the specimens by means of waterjet cutting – see Fig. 10(b). A typical sectioned residual stress specimen is shown in Fig. 11. Following the sectioning process, the final gauge length of each strip, denoted as r_f, was determined as the mean value of three subsequent readings taken on each set of gauge holes. Note that, in order to minimise the influence of any temperature changes on the measured gauge lengths, a temperature reference bar was employed, with readings taken before and after sectioning, denoted as t_i and t_f, respectively.

5. Measured residual stresses

The relieved strain ε of each strip was calculated according to Eq. (1), where r_i and r_f are the average values of the measurements taken on each strip before and after sectioning respectively, t_i and t_f are the average values of the measurements taken on the reference temperature bar before and after sectioning respectively, and L_0 is the nominal gauge length (i.e. the nominal initial distance between each pair of gauge holes), set to 250 mm. Note that a positive relieved strain ε calculated in line with Eq. (1) corresponds to a compressive residual stress, while a negative ε value indicates a tensile residual stress.

$$\varepsilon = \frac{(r_f - t_f) - (r_i - t_i)}{L_0 + r_i - t_i} \tag{1}$$

Strip curvature arising after sectioning can induce errors in the calculated residual stresses, due to the final readings over the gauge length being taken along the chord (rather than the arc) length [43] – see Fig. 12(a). Thus, the curvature of all strips was measured in the planes normal and parallel to the strip surface (i.e. planes *xz* and *xy* as per Fig. 13) using a curvature dial – see Fig. 12(b).

As usually observed in hot-rolled and welded steel sections, most of the released strips exhibited no significant curvature in the longitudinal direction – see Fig. 13(b), indicating no significant through-thickness variation in the residual stresses. This observation was corroborated by determining the bending (through thickness) residual stresses using Eq. (2), following the procedure described by Cruise and Gardner [3]. In Eq. (2), E is the Young's modulus of the material, y is the distance between the surface and the neutral axis of the strips (taken as $t/2$, where t is the material thickness) and ΔR is the change in the radius of curvature of the strip before and after sectioning. The magnitude of the bending residual stresses was found to be minimal, with the calculated σ_b values being equal to about $0.03f_y$ on average.

$$\sigma_b = \frac{Ey}{\Delta R} \tag{2}$$

It should be mentioned that some strips extracted from near the flange tips, which were in close proximity to the WAAM stiffeners, exhibited curvature in the plane parallel to the strip surface after sectioning – see Fig. 13(c); this is attributed to the steep temperature gradient induced during WAAM.

The influence of the measured curvatures on both planes (i.e. planes *xz* and *yx* as per Fig. 13) on the resulting released strains was eliminated using Eq. (3), where δ_y and δ_z are the maximum deviations of the strip from a straight line between the gauge points along y and z axes respectively (as shown in Fig. 13). Note that the curvature corrections were neglected for values of δ_y and δ_z lower than $0.001L_0$ [33,40].

$$\varepsilon_c = \varepsilon + \frac{(\delta_y/L_0)^2}{6(\delta_y/L_0)^4 + 1} + \frac{(\delta_z/L_0)^2}{6(\delta_z/L_0)^4 + 1} \tag{3}$$

The residual stresses were subsequently determined using Hooke's

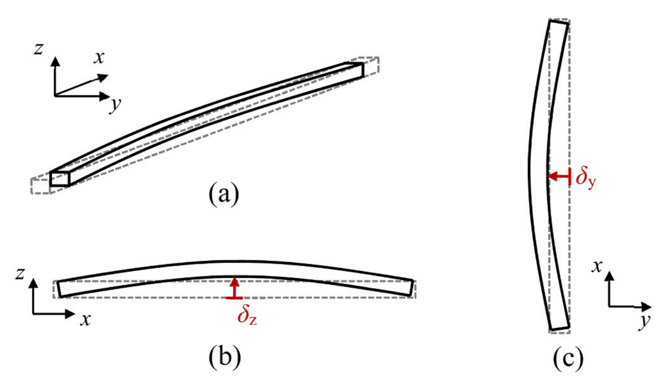

Fig. 13. Strip curvature: (a) overall view, (b) elevation, (c) plan view.

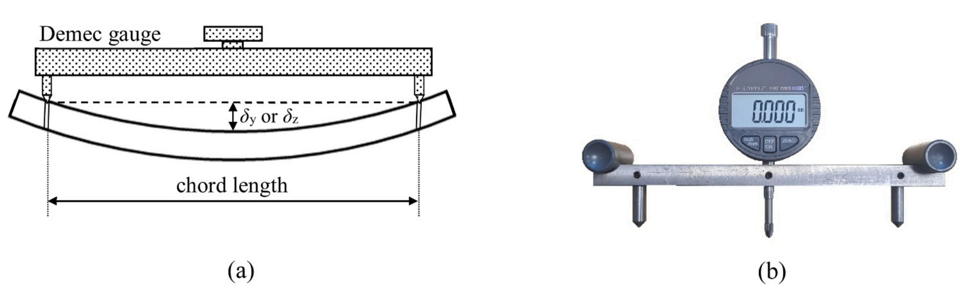

Fig. 12. (a) Measurements along chord length and (b) curvature dial.

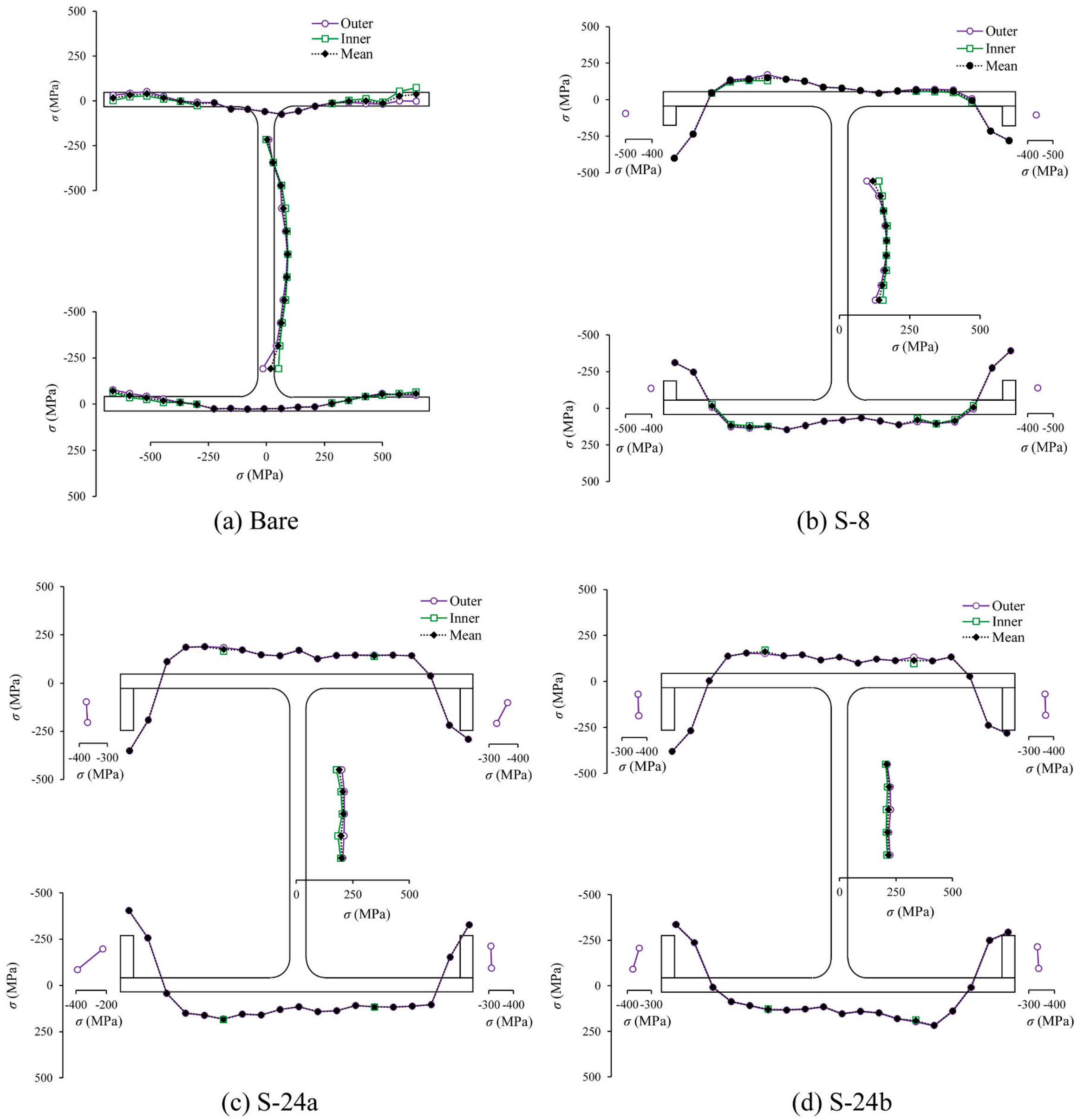

Fig. 14. Measured residual stress distributions in bare and WAAM-stiffened I-section profiles (positive = compression, negative = tension).

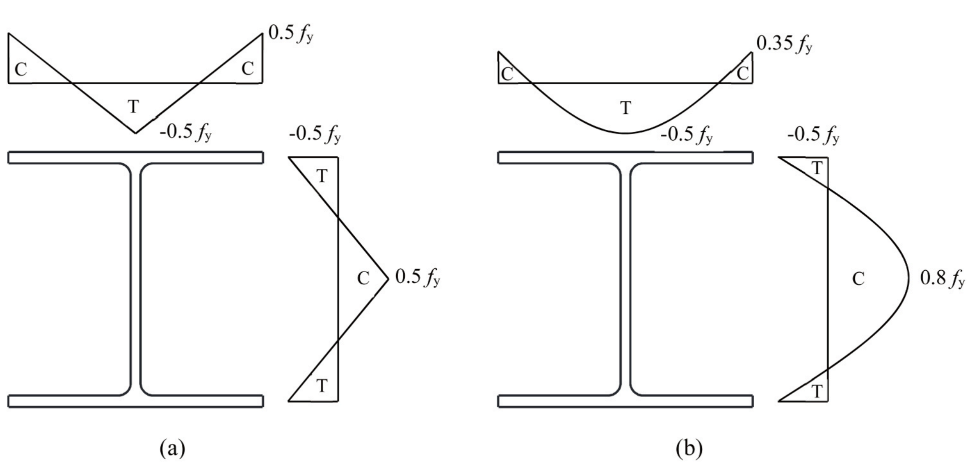

Fig. 15. Typical residual stress distributions in hot-rolled I-sections: (a) [6] and (b) [1].

Table 7
Summary of peak residual stresses in the examined cross-sections.

Specimen ID	f_{ft}/f_y	f_{fc}/f_y	f_{wc}/f_y
B	0.19	0.10	0.23
S-8	0.97	0.37	0.41
S-24a	0.98	0.45	0.50
S-24b	0.92	0.53	0.53

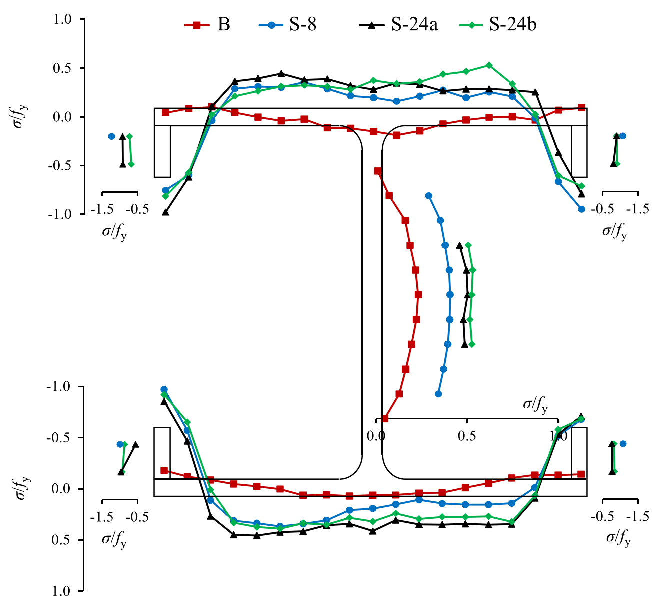

Fig. 16. Summary of measured residual stress distributions, normalised by yield strength (positive = compression, negative = tension).

law, by multiplying the released strains ε_c by the Young's modulus of the hot-rolled or WAAM steel material, as reported in Tables 5 and 6 respectively, given that any dimensional changes caused by the stress relaxation occurring after sectioning are elastic [33].

The resulting residual stress data for the examined specimens are presented in Fig. 14, where the measurements from both strip sides (i.e. the inner and outer surfaces) are plotted, along with their mean values. For all specimens, cross-section self-equilibrium was generally satisfied, with the differences between the total tensile and compressive forces being less than 5%. For the bare steel section, shown in Fig. 14(a), the magnitude of the compressive residual stresses at the flange tips was found to be equal to about 0.1 f_y, which is lower than the typical range of magnitudes (i.e. 0.35 f_y - 0.50 f_y) reported in the literature – see Fig. 15 [1,6]. Also, the residual stress distribution in the bottom flange of the bare profile was found to not follow the expected pattern for hot-rolled I-sections (i.e. compression at the flange tips and tension at the web-to-flange junction); this may be due to the effects of straightening of the member during production through plastic deformation, which is common practice to ensure that geometric tolerances are met, and has been shown to lead to alterations to the residual stress pattern in I-sections [15,38].

As can be observed in Fig. 14(b)-(d), all WAAM-strengthened specimens exhibited consistently high tensile residual stresses in the stiffeners and at the flange tips, with self-equilibrating compressive residual stresses elsewhere. This represents a more favourable residual stress distribution in terms of member stability behaviour, particularly for minor axis flexural buckling, as demonstrated by Gardner et al. [12]. Similar residual stress patterns are seen in welded I-sections fabricated from plates with flame-cut edges [41].

It was found that the maximum measured tensile residual stresses in the WAAM stiffeners of Specimen S-8 were higher than those in Specimens S-24a and S-24b, suggesting that the maximum tensile residual stresses reduce with increasing stiffener height. This can be explained by the fact that the column shortens as successive layers of WAAM material are added and contract upon cooling, thus slightly relieving the tensile residual stresses in the preceding layers.

The obtained residual stress distributions in the WAAM-strengthened sections appear to be essentially insensitive to the underlying residual stress pattern in the bare profile, as evidenced by the largely symmetric distributions shown in Fig. 14(b) to (d), despite the asymmetry seen in Fig. 14(a). The measured variation in residual stress through the thickness of the sections was minor in all cases. Note that, although for deep, slender webs, the increased compressive residual stresses within the web of the strengthened sections could cause a reduction in local buckling capacity, it is not anticipated that this would be the case for hot-rolled steel sections of typical proportions.

The peak tensile and compressive residual stresses in the flanges and web of the examined sections are reported in Table 7, normalised by the average yield strength f_y of the material while, in Fig. 16, a summary of the distributions is presented in the same normalised format. In Table 7, the subscripts "f", and "w" refer to the flange and web respectively, while "t" and "c" denote tension and compression, respectively. The magnitudes of the tensile residual stresses generated at the flange tips due to the thermal prestressing induced through the WAAM process were found to be almost equal to f_y for all strengthened specimens (varying between 0.92f_y and 0.98f_y), irrespective of the height of the stiffener. It can thus be concluded that the addition of even a small amount of WAAM material at the flange tips, corresponding to a small increase in the total mass of the specimen, is sufficient to create the desirable tensile residual stresses in the vicinity of the stiffeners.

The described favourable residual stress pattern, in combination with the increased area and second moment of area and the enhanced local buckling resistance provided by the WAAM stiffeners, has been shown to lead to substantial capacity increases in the case of hot-rolled steel I-section columns buckling about the minor axis. Specifically, increases in axial capacity of between 17% and 54% were achieved for increases in mass of between 2% and 26% [12]. Considered in isolation, the structural efficiency of the WAAM stiffener material (measured in terms of load-carrying capacity per unit mass) was between about two and eight times that of the bare steel section, representing significant savings in both raw material and embodied carbon [30].

6. Conclusions

The concept of hybrid structural elements of enhanced structural efficiency featuring hot-rolled steel I-sections strengthened by WAAM stiffeners has been introduced. WAAM stiffeners printed onto I-sections can improve their structural performance through an increased cross-sectional area and second moment of area, enhanced local buckling capacity and a more favourable residual stress pattern; the latter has been the focus of this paper. An experimental investigation has been undertaken to determine the residual stress distribution arising through the addition of WAAM stiffeners at the flange tips of I-sections. Residual stress distributions in one bare steel I-section and three WAAM-strengthened I-sections with different stiffener heights were determined using the sectioning method. The results of complementary material tests, undertaken to determine the mechanical properties of the hot rolled and WAAM steels (i.e. the I-section and stiffeners, respectively), were also presented. The adopted experimental techniques have been described in detail, while the magnitude and distribution of the residual stresses have been presented. It is shown that the heat input induced during WAAM inverts the typical detrimental residual stress pattern associated with hot-rolled steel I-sections, which has compressive residual stresses at the flange tips, replacing it with a substantially more desirable residual stress pattern (in terms of structural stability) with tension at the flange tips. It was further found that only a small amount of added material is required to achieve the described beneficial effects. The presented findings highlight the significant enhancements in terms of structural efficiency, material savings and reduction in environmental impact that can be achieved by the use of the described hybrid manufacturing concept, opening up opportunities for the strengthening and repair of new and existing infrastructure.

Declaration of Competing Interest

The authors declare that they have no known competing financial interests or personal relationships that could have appeared to influence the work reported in this paper.

Acknowledgements

The authors would like to thank Steelo Ltd for providing the test specimens.

References

[1] Bradford MA, Trahair NS. Inelastic buckling of beam-columns with unequal end moments. J Constr Steel Res 1985;5:195–212.
[2] Colegrove PA, Coules HE, Fairman J, Martina F, Kashoob T, Mamash H, et al. Microstructure and residual stress improvement in wire and arc additively manufactured parts through high-pressure rolling. J Mater Process Technol 2013;213(10):1782–91.
[3] Cruise RB, Gardner L. Residual stress analysis of structural stainless steel sections. J Constr Steel Res 2008;64:352–66.
[4] Davis 10 (Version 10.1.1) [Software] La Vision GmbH, 2017.
[5] Ding J, Colegrove P, Mehnen J, Ganguly S, Almeida PS, Wang F, et al. Thermo-mechanical analysis of Wire and arc additive layer manufacturing process on large multi-layer parts. Comput Mater Sci 2011;50(12):3315–22.
[6] ECCS. Ultimate limit state calculations of sway frames with rigid joints. Technical Committee 8 – Structural Stability Technical Working Group 8.2 [First Edition]. Belgium, Brussels: ECCS Publications; 1984.
[7] EN ISO 14341:2020 Welding consumables – Wire electrodes and weld deposits for gas shielded metal arc welding of non alloy and fine grain steels – Classification. European Committee for Standardization, Brussels, 2020.
[8] EN ISO 6892-1:2016 Metallic materials – tensile testing – Part 1: method of test at room temperature. European Committee for Standardization, Brussels, 2016.
[9] Gardner L. Metal additive manufacturing in structural engineering – review, advances, opportunities and outlook. Structures 2023;47:2178–93.
[10] Gardner L, Cruise RB. Modeling of residual stresses in structural stainless steel sections. J Struct Eng ASCE 2009;135(1):42–53.
[11] Gardner L, Bu Y, Theofanous M. Laser-welded stainless steel I-sections: Residual stress measurements and column buckling tests. Eng Struct 2016;127:536–48.
[12] Gardner L, Li J, Meng X, Huang C, Kyvelou P. I-section steel columns strengthened by additive manufacturing. Concept Exp Eng Struct 2023 ([Submitted]).
[13] Geomagic Wrap. [Software] 3D Systems, Inc; 2017.
[14] Gu J, Ding J, Williams SW, Gu H, Bai J, Zhai Y, et al. The strengthening effect of inter-layer cold working and post-deposition heat treatment on the additively manufactured Al–6.3 Cu alloy. Mater Sci Eng A 2016;651:18–26.
[15] Guan B, Zang Y, Wu D, Qin Q. Stress-inheriting behavior of H-beam during roller straightening process. J Mater Process Technol 2017;244:253–72.
[16] Guo X, Kyvelou P, Ye J, Teh LH, Gardner L. Experimental investigation of wire arc additively manufactured steel single-lap shear bolted connections. Thin-Walled Struct 2022;181:110029.
[17] Hönnige JR, Colegrove PA, Ahmad B, Fitzpatrick ME, Ganguly S, Lee TL, et al. Residual stress and texture control in Ti-6Al-4V wire+ arc additively manufactured intersections by stress relief and rolling. Mater Des 2018;150:193–205.
[18] Hönnige JR, Colegrove PA, Ganguly S, Eimer E, Kabra S, Williams S. Control of residual stress and distortion in aluminium wire + arc additive manufacture with rolling. Addit Manuf 2018;22:775–83.
[19] Huang C, Meng X, Gardner L. Cross-sectional behavior of wire arc additively manufactured tubular beams. Eng Struct 2022;272:114922.
[20] Huang C, Kyvelou P, Gardner L. Stress-strain curves for wire arc additively manufactured steels. Eng Struct 2023;279:115628.
[21] Huang C, Kyvelou P, Zhang R, Britton TB, Gardner L. Mechanical testing and microstructural analysis of wire arc additively manufactured steels. Mater Des 2022;216:110544.
[22] Huang W, Wang Q, Ma N, Kitano H. Distribution characteristics of residual stresses in typical wall and pipe components built by wire arc additive manufacturing. J Manuf Process 2022;82:434–47.
[23] Kanyilmaz A, Demir AG, Chierici M, Berto F, Gardner L, Kandukuri SY, et al. Role of metal 3D printing to increase quality and resource-efficiency in the construction sector. Addit Manuf 2022;50:102541.
[24] Martina F, Roy MJ, Szost BA, Terzi S, Colegrove PA, Williams SW, et al. Residual stress of as-deposited and rolled wire+ arc additive manufacturing Ti–6Al–4V components. Mater Sci Technol 2016;32(14):1439–48.
[25] Meng X, Weber B, Nitawaki M, Gardner L. Optimisation and testing of wire arc additively manufactured steel stub columns. Thin-Walled Struct 2023;189:110857.
[26] Quach WM, Teng JG, Chung KF. Residual stresses in press-braked stainless steel sections, I: coiling and uncoiling of sheets. J Constr Steel Res 2009;65(8-9):1803–15.
[27] Quach WM, Teng JG, Chung KF. Residual stresses in press-braked stainless steel sections, II: press-braking operations. J Constr Steel Res 2009;65(8-9):1816–26.
[28] Rhino 3D. (Version 5 SR14 64-bit) 607 [Software] Robert McNeel & Associates; 2017.
[29] Schajer GS. Practical residual stress measurement methods. West Sussex, UK: John Wiley & Sons Ltd; 2013.
[30] Shah IH, Hadjipantelis N, Walter L, Myers RJ, Gardner L. Environmental life cycle assessment of wire arc additively manufactured structural components. J Clean Prod 2023;389:136071.
[31] Shen H, Lin J, Zhou Z, Liu B. Effect of induction heat treatment on residual stress distribution of components fabricated by wire arc additive manufacturing. J Manuf Process 2022;75:331–45.
[32] Su A, Sun Y, Liang Y, Zhao O. Membrane residual stresses and local buckling of S960 ultra-high strength steel welded I-section stub columns. Thin-Walled Struct 2021;161:107497.
[33] Tebedge N, Alpsten G, Tall L. Residual-stress measurement by the sectioning method. Exp Mech 1973;73033:88–96.
[34] Withers PJ, Bhadeshia HK. Residual stress: part 1 – measurement techniques. Mater Sci Technol 2001;17(4):355–65.
[35] Withers PJ, Bhadeshia HK. Residual stress. Part 2 – nature and origins. Mater Sci Technol 2001;17(4):366–75.
[36] Wu Q, Mukherjee T, De A, DebRoy T. Residual stresses in wire-arc additive manufacturing–hierarchy of influential variables. Addit Manuf 2020;35:101355.
[37] Xiong J, Lei Y, Li R. Finite element analysis and experimental validation of thermal behavior for thin-walled parts in GMAW-based additive manufacturing with various substrate preheating temperatures. Appl Therm Eng 2017;126:43–52.
[38] Yin J, Zhao J, Wang S, Li Y, Li Y. Multiroller straightening analytical model of H-beam. Ironmak Steelmak 2013;41(7):521–8.
[39] Young BW. Residual stresses in hot rolled members. IABSE reports of the working commissions. Zürich, Switzerland: ETH Zürich; 1975.
[40] Yuan HX, Wang YQ, Shi YJ, Gardner L. Residual stress distributions in welded stainless steel sections. Thin-Walled Struct 2014;79:38–51.
[41] Yun X, Zhu Y, Meng X, Gardner L. Welded steel I-section columns: residual stresses, testing, simulation and design. Eng Struct 2023;282:115631.
[42] Zheng B, Yang S, Jin X, Shu G, Dong S, Jiang Q. Test on residual stress distribution of welded S600E high-strength stainless steel sections. J Constr Steel Res 2020;168:105994.
[43] Ziemian RD. Guide to stability design criteria for metal structures. New Jersey, US: John Wiley & Sons Inc; 2010.